

Article

Synthesis, Characterization, and Properties of a Novel Hyperbranched Polymers with Polyacrylamide Side Chains

Xiaoping Qin ¹, Qianwen Wang ¹, Peng Tang ^{1,2,*}, Hui Yang ³, Cuixia Li ¹, Xiaoliang Yang ³ and Tong Peng ³

¹ School of Chemical Engineering, Sichuan University of Science and Engineering, Zigong 643000, China; 13568322767@163.com (X.Q.); 18982607289@163.com (Q.W.); licuixia2023@126.com (C.L.)

² Tianjin Key Laboratory of Brine Chemical Engineering and Resource Eco-Utilization, College of Chemical Engineering and Materials Science, Tianjin University of Science and Technology, No. 29, 13th Street, Binhai New District, Tianjin 300457, China

³ Jidong Oilfield Branch Company, PetroChina Company Limited, Tangshan 063002, China; yanghui2023jd@outlook.com (H.Y.); yangmeimei178@163.com (X.Y.); jd_pengtong@petrochina.com.cn (T.P.)

* Correspondence: tpdzyyx@163.com

Abstract: A novel hyperbranched polymer with polyacrylamide side chains (HAPAM) was synthesized by aqueous solution polymerization using acrylic acid, acrylamide, 2-acrylamido-2-methyl-1-propanesulfonic acid, hydrophobic monomer of dimethyl octadecyl ammonium chloride, and the homemade skeleton monomer of modified-M_{2,0} as raw materials and (NH₄)₂S₂O₈-NaHSO₃ as initiator. The molecular structure, functional groups, and surface morphology of HAPAM were characterized by Fourier transform infrared spectroscopy, nuclear magnetic resonance hydrogen spectroscopy, and scanning electron microscopy. It was found that the performance of HAPAM solution was higher than that of ordinary polyacrylamide solution in terms of thickening ability, shearing resistance, thermal endurance, salt-resistance, resistance-coefficient and residual-resistance-coefficient, ability to reduce interfacial tension between polymer solution and crude oil, and oil-displacement-efficiency. In particular, the enhanced oil recovery of the HAPAM solution was 13.03%, and the improvement of shearing resistance and immunity to chromatographic separation were simultaneously achieved by the HAPAM solution. These results indicate that the successful synthesis of the novel HAPAM opens a promising strategy for developing new high-performance oil-displacing polymers.

Keywords: hyperbranched polymers; amphiphilic polyacrylamide; polymerization; thickening ability; enhanced oil recovery



Citation: Qin, X.; Wang, Q.; Tang, P.; Yang, H.; Li, C.; Yang, X.; Peng, T. Synthesis, Characterization, and Properties of a Novel Hyperbranched Polymers with Polyacrylamide Side Chains. *Materials* **2024**, *17*, 1619.

<https://doi.org/10.3390/ma17071619>

Academic Editors: Edward Bormashenko and Abderrahim Yassar

Received: 12 January 2024

Revised: 9 March 2024

Accepted: 14 March 2024

Published: 1 April 2024



Copyright: © 2024 by the authors. Licensee MDPI, Basel, Switzerland. This article is an open access article distributed under the terms and conditions of the Creative Commons Attribution (CC BY) license (<https://creativecommons.org/licenses/by/4.0/>).

1. Introduction

After the first and second stages of oil production from the well, there were still large volumes of the original oil bypassed or trapped in the reservoir [1–3]. Therefore, enhanced oil recovery (EOR) methods were used to recover the additional oil [4–7]. The EOR methods were majorly classified into thermal and non-thermal EOR [8–10]. Unfortunately, thermal EOR methods were unsuitable for reservoirs with great depth and thin pay zones [11]. In addition, the application of thermal EOR was still challenged both economically and environmentally because of the high cost of heat supply along with excessive CO₂ emission and costly post-treatment and maintenance [12,13]. Hence, non-thermal EOR methods, including physical, chemical, and biological techniques [14], have received prodigious attention in the recovery of conventional and heavy oil [15]. Amongst all non-thermal EOR methods, chemical EOR has been recognized as the most promising technique due to its technical and economic feasibility and reasonable capital cost [16]. Polymer flooding was the simplest and most widely used chemical EOR process [17].

Because of the synergistic improvement of sweep efficiency and oil-washing efficiency, binary polymeric surfactant mixtures (BPSMs) have become the main chemical EOR technique for recovering the oil in oilfields with high and ultra-high water cuts [18,19].

However, the on-site applications were still severely inhibited due to two major technical bottlenecks. First, the extensively used BPSMs (such as partially hydrolyzed linear polyacrylamide, PAM) still have relatively poor shear resistance [20], and their sweeping efficiency and oil-washing efficiency were low [21], which need to be further advanced. Second, the synergistic effect of BPSMs was significantly weakened by chromatographic separation (i.e., the differential transport speed of BPSMs flowing in the boreholes after injection into the stratum). Therefore, it is necessary to improve the poor shear resistance and avoid the chromatographic separation of BPSMs to further advance their oil-displacing performance [22,23].

In recent years, several research groups reported that oil-displacing polymers with special molecular structures (comb-type [24], star-type [25], and hyperbranched type [26]) show strong shear resistance [27,28]. Duan et al. [29] studied the flow-induced scission behavior of PAM with four-arm-star during planar elongational flow in a cross-slot flow cell. They also found that the PAM with a four-arm star exhibited better-shearing stability than that of the linear PAM at the same shearing rate. Chen et al. [30] synthesized a new type of chitosan-modified hyperbranched polymers (HPDACs) by the free-radical polymerization of surface-modified chitosan with acrylic acid (AA) and acrylamide (AM). After mechanical shearing, the viscosity retention rate of HPDACs in ultrapure water and simulated brine was higher than that of PAM and the dendritic polymer, indicating the excellent shear resistance and good viscoelasticity of HPDACs. In addition, in order to effectively avoid chromatographic separation problems of BPSMs, both hydrophobic and hydrophilic groups were introduced into BPSMs [31] to improve the ability to expand the swept volume and oil displacing efficiency [32,33]. Zhu et al. [34] synthesized an amphiphilic polymer with twin-tailed hydrophobic groups (TAP). They estimated a lower critical aggregation concentration (CAC, 800 mg/L) of TAP, and a higher apparent viscosity can be obtained when the concentration of TAP was higher than CAC due to the strong hydrophobic association. However, to date, there have been limited reports about hyperbranched amphiphilic polyacrylamides (HAPAMs) with synergistic effects of excellent shearing resistance and a strong ability to reduce interfacial tension [35–40]. To this end, in this work, a novel HAPAM with 16 branched chains was successfully synthesized by introducing hydrophobic group (dimethyl octadecyl ammonium chloride, DMCAAC-18) and hydrophilic groups (AA, AM, and AMPS, abbreviated from 2-acrylamido-2-methyl-1-propanesulfonic acid) into the molecular chain, simultaneously enhancing the shear-resistance and avoiding the phenomenon of chromatographic separation. Their microstructures, functional groups, and surface morphology were characterized using Fourier transform infrared spectroscopy (FT-IR), nuclear magnetic resonance hydrogen spectroscopy ($^1\text{H-NMR}$), and scanning electron microscopy (SEM). The differences between HAPAM and PAM on thickening ability, shear-resistance, temperature resistance, salt resistance, resistance-coefficient and residual-resistance-coefficient, ability to reduce interfacial tension, and oil-displacement-efficiency were investigated via a series of systematic tests.

2. Experimental Section

2.1. Materials

All chemicals used in this study were of analytical grade and were used without any further purification. Acrylamide (AM), acrylic acid (AA), sodium hydroxide, sodium bicarbonate, ethanol, sodium chloride, potassium chloride, sodium bisulfite (SDS), ethylene-diamine (EDA), methanol, methyl acrylate (MA), N,N-Dimethylformamide (DMF), Maleic anhydride (MAH) and anhydrous sodium sulfate were purchased from Chengdu Kelong Chemical Co., Ltd. (Chengdu, China). 2-acrylamido-2-methyl-1-propane sulfonic acid (AMPS) was purchased from Bide Pharmatech Co., Ltd. (Shanghai, China) Ammonium persulfate was supplied by Guangdong Guanghua Sci-Tech Co., Ltd. (Shantou, China). Anhydrous magnesium chloride was purchased from Tianjin Balance Bio-tech Co., Ltd. (Tianjin, China). Calcium chloride was supplied by Chengdu Jinshan Chemical Reagent Co., Ltd. (Chengdu, China). Dodecyl dimethyl allyl ammonium chloride (DMDAAC-18)

was bought from Zhangjiagang Renda Chemical Co., Ltd. (Suzhou, China). And ammonium persulfate (APS) was supplied by Guangdong Guanghua Sci-Tech Co., Ltd. (Shantou, China). Especially, the composition of the simulated injection-water was given in Table 1.

Table 1. Compositions of ions in the simulated injection water.

Ions	Na ⁺	K ⁺	Ca ²⁺	Mg ²⁺	HCO ₃ [−]	SO ₄ ^{2−}	Cl [−]
Concentrations (mg/L)	667	28	20	13	379	68	870

2.2. Synthesis Processes

2.2.1. Synthesis of Modified-M_{2.0}

As described in the reference [41], the skeleton-polymer of a 2.0 generation dendritic macromolecule (M_{2.0}) with eight branch chains was synthesized as follows steps. Step (i), 18.0 g of ethylenediamine (EDA) and 60 g of methanol were added into a three-necked flask with a magnetic stirrer for stirring, a reflux condenser for reflux condensation, and a thermometer for temperature-monitoring. In addition, 113.2 g of methyl acrylate (MA) was gradually dripped into the solution. The reaction was controlled at 25 ± 0.1 °C for 24 h. After the reaction, M_{0.5} was purified and obtained by vacuum distillation and silica gel column. Step (ii), 40.4 g of M_{0.5} and 64 g of methanol were added into a fresh three-necked flask with a magnetic stirrer, reflux condenser, and thermometer, dripping with 80 g of EDA. The reaction of the stirring solution was controlled at 72 ± 0.1 °C for 24 h. After the reaction, M_{1.0} was purified and obtained by vacuum distillation and silica gel column. Step (iii), 30 g of M_{1.0} and 40 g of methanol were added into a fresh three-necked flask with a magnetic stirrer, a reflux condenser tube, and a thermometer, with dripping 50 g of MA. The reaction of the stirring solution was controlled at 72 ± 0.1 °C for 24 h. After the reaction, M_{1.5} was purified and obtained by vacuum distillation and silica gel column. Step (iv), 30 g of M_{1.5} and 50 g of methanol to a fresh three-necked flask with a magnetic stirrer, reflux condenser tube, and a thermometer, dripping with 14 g of EDA. The reaction of the stirring solution was also controlled at 72 ± 0.1 °C for 24 h. Finally, the dendritic skeleton-polymer of M_{2.0} was purified and obtained by vacuum distillation and silica gel column. Step (v) was the process of modifying the structure of M_{2.0}. 8 g of M_{2.0} and 30 g of N, N-Dimethylformamide (DMF) were added into a beaker to dissolve M_{2.0} completely, slowly dripping with 4.4 g of maleic anhydride. After finishing the addition of maleic anhydride (MAH), the beaker was sealed and put into an oven to react at 70 °C for 6 h. In the end, the solution of the modified-M_{2.0} was obtained in the form of a brown transparent solution. Especially, the synthetic yield of M_{0.5}, M₁, M_{1.5}, and M₂ was 93.3%, 95.5%, 95.8%, and 96.1%, respectively. Additionally, there one work reported that the synthetic yield of M_{0.5}, M₁, M_{1.5}, and M₂ was 98.1%, 98.7%, 99.2%, and 99.7%, respectively [42]. Therefore, this similarity indirectly implied the accuracy of our experiments.

2.2.2. Synthesis of HAPAM and PAM

To enable the dendritic skeleton to participate in polymerization, cis-butenedioic anhydride was used to introduce double bonds into the modified dendritic M_{2.0}. Then, the detailed synthesis process of HAPAM was given as follows: a round bottom flask with three necks was added with 30 g of deionized water and 6.0 g of AA and deaerated by N₂. NaOH was added into the solution to adjust pH = 7 after the complete dissolution of AA. Besides, the solution was added with 6.1 g of AM, 0.5 g of AMPS, 1.2 g of DMCAAC-18, and 0.5 g of M_{2.0}, respectively, stirring until complete dissolution. Again, deionized water was added to adjust the mass concentration (25 wt%) of AM, AMPS, DMCAAC-18, and M_{2.0} in the whole solution. The temperature of the solution was stabilized at 40 °C, gradually adding (NH₄)₂S₂O₈ and NaHSO₃ (0.2 wt% and molar ratio of (NH₄)₂S₂O₈ and NaHSO₃ was 1:1) as an initiator with stirring evenly. Finally, the above mixtures were sealed in a beaker for reaction about 4 h to obtain HAPAM. The synthesis formula of D-M-HPA is shown in

Figure 1. The PAM was prepared using the same method without adding DMCAAC-18 and $M_{2.0}$.

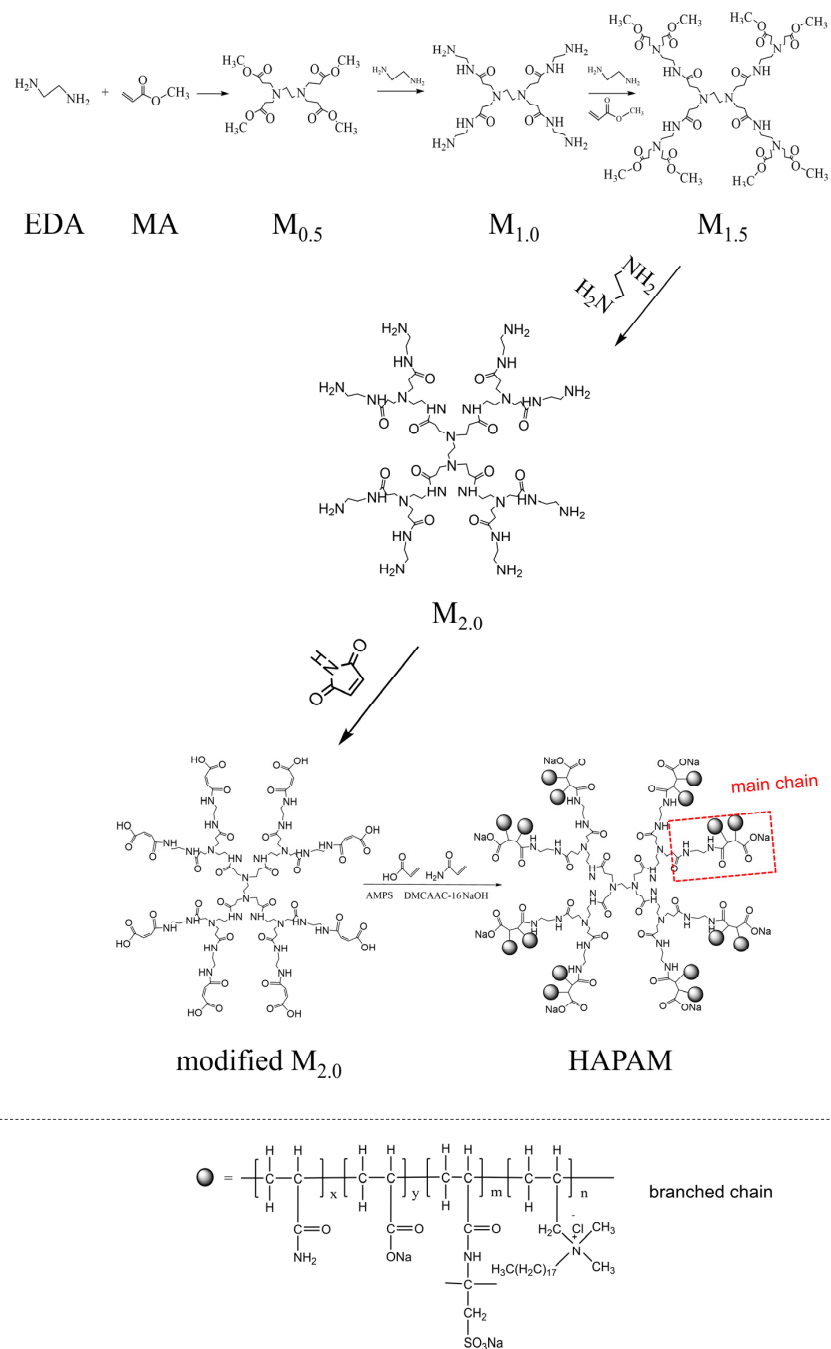


Figure 1. Synthetic route and structure of HAPAM.

2.3. Characterization

The microstructures of HAPAM and PAM were characterized by a VEGA3SBU scanning electron microscope (SEM, Beijing Dongxiyi Technology Co., Ltd., Beijing, China). The sample preparation for SEM was given as follows: (i) the concentration of both PAM solution and HAPAM polymer solution was 1000 mg/L, (ii) 1-2 drops of the solutions were taken onto the conductive adhesive and treated in a vacuum freeze-drying oven for 24 h, (iii) after gold spraying, the samples were observed by scanning electron microscopy. The infrared spectrum of HAPAM was measured by a Fourier infrared spectrometer (FTIR-650, Tianjin Zhongke Ruijie Technology Co., Ltd., Tianjin, China). HAPAM was characterized

by an FTIR-650 Fourier infrared spectrometer. The sample preparation for FTIR was given as follows: (i) Wash HAPAM with anhydrous ethanol three times, (ii) put it in the oven at 35 °C to get a solid with a crisp texture, (iii) take it out and grind it into powder, (iv) evenly disperse the ground fine powder in potassium bromide and press it into a transparent sheet sample, (v) KBr should be dried before use, and the grinding particle size was less than 2 microns. The ¹H-NMR spectrum of HAPAM was obtained by a nuclear magnetic resonance instrument (Bruker-AC-E200, Bruker, Switzerland). The sample preparation for 1H-NMR was given as follows: (i) Clean HAPAM with anhydrous ethanol 3 times to remove impurities, (ii) put it in a vacuum drying oven at 35 °C for drying, (iii) take it out and grind it into a fine powder after drying, (iv) put 1–2 mg into a nuclear magnetic tube, and (v) use 0.55 mL D₂O to completely dissolve it.

2.4. Performance-Evaluation

The difference between HAPAM and PAM on thickening ability, shear-resistance, thermal endurance, and salt-resistance were evaluated via a series of static tests by measuring the apparent viscosity of HAPAM and PAM solutions using an NDJ-5S digital rotary viscometer rotor at the speed of 30 rpm (Shanghai Fangrui Instrument Co., Shanghai, China). Additionally, the interfacial tension of HAPAM and PAM solutions (with mass concentrations of 500 mg/L, 750 mg/L, and 1000 mg/L) was measured by the interfacial tension meter (Guangdong Insa Instrument Technology Co., Dongguan, China). The resistance-coefficient and residual-resistance-coefficient for 2000 mg/L of HAPAM and PAM solutions were determined using sandpack core flooding experiments at 65 °C. The sand pack core holder (Φ2.5 cm × 30 cm) was filled with quartz sand of 80–120 meshes (with a porosity of 36.69%). Before oil injection, the packed core was vacuumed with a vacuum pump to drain the core and saturated water completely. Then, the initial water permeability of the sand pack core was measured, and the porosity of the core could be calculated according to the volume of the brine absorbed by the vacuumed porous media. In addition, crude oil was injected into the sand pack core until the brine production became negligible. Secondly, the specific experimental steps of water flooding and polymer flooding were given as follows: (1) Water-driving-stage: the sand pack core holder was injected with the simulated injection water at an injection speed of 10 mL/min, recording the stabilized pressure of P_{w1} (MPa). (2) Polymer-flooding-stage: 2000 mg/L of HAPAM or PAM solutions were injected into the one-dimensional sand-filling model at an injection rate of 10 mL/min, also recording the stabilized pressure of P_p (MPa). (3) Subsequent-water-driving stage: the one-dimensional sand-filling model was injected with the simulated injection water again at an injection speed of 10 mL/min, recording the stabilized pressure of P_{w2} (MPa). The resistance-coefficient (RF) and residual-resistance-coefficient (RRF) can be given as the following formula.

$$RF = \frac{P_p}{P_{w1}} \quad (1)$$

$$RRF = \frac{P_{w2}}{P_{w1}} \quad (2)$$

Moreover, the oil-displacement performance of HAPAM or PAM solutions (2000 mg/L) was also determined by the sand pack core flooding experiments. The detailed experimental steps are as follows: (1) The sand pack core holder was saturated with the simulated injection water, as given in Table 1 (water-flooding). (2) Then, it was saturated with crude oil (778.56 mPa·s) at a speed of 2 mL/min (polymer-flooding) until irreducible water saturation. After aging for 24 h, the simulated injection water was injected at a speed of 2 mL/min to displace the crude oil until the water cut reached above 95%. Again, the polymer solution was injected at a speed of 2 mL/min to obtain a water cut that reached above 95%. The EOR of the polymer solutions can be calculated by the following equation:

$$EOR = E_{total} - E_{water} \quad (3)$$

where EOR , E_{total} , and E_{water} were EOR of polymer solution (%), oil recovery of water-flooding and polymer-flooding process (%), and oil recovery of water-flooding process (%).

3. Results and Discussion

3.1. Infrared Spectrum of $M_{0.5}$, $M_{1.0}$, $M_{1.5}$, $M_{2.0}$, and HAPAM

The IR spectra of $M_{0.5}$, $M_{1.0}$, $M_{1.5}$, $M_{2.0}$, and HAPAM were given in Figure 2, and the peaks were also given in Table 2, respectively. For $M_{1.0}$, $M_{1.5}$, and $M_{2.0}$, the peaks near $3288\sim 3295\text{ cm}^{-1}$ and $3068\sim 3078\text{ cm}^{-1}$ can be ascribed to N-H stretching vibration [43,44], while the strong peak of HAPAM near 3433 cm^{-1} can be assigned to the multiple complex groups of its -CONH- and -CONH₂. Meanwhile, the peaks of $M_{0.5}$, $M_{1.0}$, $M_{1.5}$, $M_{2.0}$, and HAPAM around $2928\sim 2951\text{ cm}^{-1}$ and $2837\sim 2860\text{ cm}^{-1}$ were categorized as antisymmetric and symmetric stretching vibration of C-H [45,46]. The C=O stretching vibrational peaks in the group of -COOC- for $M_{0.5}$, $M_{1.0}$, $M_{1.5}$, and $M_{2.0}$ were located at relatively stronger peaks of $1727\sim 1731\text{ cm}^{-1}$ and weaker peaks of $1644\sim 1652\text{ cm}^{-1}$. Meanwhile, the C=O stretching vibrations in several groups of -CONH-, -CONH₂, and -COONa for HAPAM resulted in a strong and broad peak near 1635 cm^{-1} [47,48]. In particular, for $M_{0.5}$, $M_{1.0}$, $M_{1.5}$, $M_{2.0}$, and HAPAM, the N-H bending vibrational peaks of CONH-, the C-H in-plane bending vibrational peaks, and the C-N stretching vibrational peaks of tertiary amines were respectively appeared round $1549\sim 1477\text{ cm}^{-1}$, $1416\sim 1473\text{ cm}^{-1}$, and $1319\sim 1361\text{ cm}^{-1}$, respectively [49–51]. In addition, the stretching vibrational peaks of C-C and tertiary amine C-N were observed at $1175\sim 1199\text{ cm}^{-1}$ in $M_{0.5}$, $M_{1.0}$, $M_{1.5}$, $M_{2.0}$, and HAPAM [52]. Interestingly, the stretching vibrational peaks of C-O-C in $M_{0.5}$ and $M_{1.5}$, the stretching vibrational peaks of primary amine C-N in $M_{1.0}$ and $M_{2.0}$, the C-O bonds of -COONa in HAPAM, and the stretching vibrational peak of S=O in -SO₃Na were also overlapped at this position [53–55]. Also, tertiary amine C-N stretching vibrational peaks of $M_{0.5}$, $M_{1.0}$, $M_{1.5}$, $M_{2.0}$, and HAPAM were observed around $1123\sim 1127\text{ cm}^{-1}$ [56]. In addition, the primary amine C-N stretching vibration and N-H in-plane bending vibration stretching vibration peaks for $M_{1.0}$ and $M_{2.0}$, the C-O bond of -COONa in HAPAM, and the S-O stretching vibration peak in -SO₃Na were also overlapped around this range [57–59]. The stretching vibration peaks of tertiary amine C-N were observed at $1036\sim 1044\text{ cm}^{-1}$ for $M_{0.5}$, $M_{1.0}$, $M_{1.5}$, $M_{2.0}$ [60], and HAPAM. Meanwhile, the stretching vibration peaks of primary amine C-N and N-H in-plane bending vibration for $M_{1.0}$ and $M_{2.0}$ also overlapped around this position [61]. Thus, the strong characteristic peaks of -COONa and -SO₃Na indicated the successful synthesis of HAPAM.

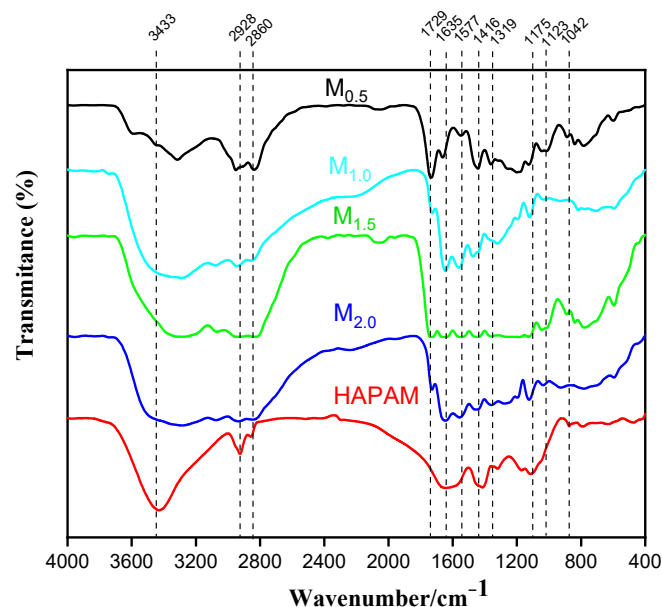


Figure 2. IR Spectrum of $M_{0.5}$, $M_{1.0}$, $M_{1.5}$, $M_{2.0}$, and HAPAM.

Table 2. Main peaks obtained from FTIR of M0.5, M1.0, M1.5, M2.0, and HAPAM.

No.	1	2	3	4	5	6	7	8	9	10	11	12	13	14
Peaks (wavelength/cm ⁻¹) of M 0.5		3315			2951	2837	1734	1662		1442	1361	1199	1126	1043
Peaks (wavelength/cm ⁻¹) of M 1.0			3290	3078	2943	2845	1727	1644	1561	1473	1321	1194	1120	1039
Peaks (wavelength/cm ⁻¹) of M 1.5			3295	3068	2946	2844	1731	1652	1549	1446	1360	1194	1127	1044
Peaks (wavelength/cm ⁻¹) of M 2.0			3288	3074	2943	2847	1729	1644	1556	1459	1359	1196	1123	1036
Peaks (wavelength/cm ⁻¹) of HAPAM	3433				2928	2860		1635	1577	1416	1319	1175	1123	1042

3.2. ¹H-NMR Spectrum of HAPAM

The ¹H-NMR spectrum of HAPAM is illustrated in Figure 3, and all the peaks have been labeled from a to l, and the positions in the HAPAM structure were indicated accordingly. **Peak a** (δ0.84) and **peak b** (δ1.24) resulted from the proton absorption peaks of -CH₃ and -(CH₂)- in the group of -N⁺-CH₂-CH₂-(CH₂)₁₅CH₃ in the hydrophobic branched chain of DMCAAC-18 [62]. **Peak c** (δ1.42) was caused by the proton absorption peak of -CH₂- $\overset{|}{\underset{|}{\text{CH}}}$ -CH₂-N⁺ in the hydrophobic branched chain of DMCAAC-18 and by the proton absorption peak of -CH₃ in the AMPS chain. **Peak d** (δ1.68) belonged to the proton absorption peak of -CH₂- $\overset{|}{\underset{|}{\text{CH}}}$ -CONH₂ [63], -CH₂- $\overset{|}{\underset{|}{\text{CH}}}$ -CONH-, -CH₂- $\overset{|}{\underset{|}{\text{CH}}}$ -COONa, and -CH₂-CH₂-(CH₂)₁₅CH₃ in the chain of AA, AM, AMPS, and hydrophobic branched chain of DMCAAC-18. **Peak e** (δ2.08) was assigned to the proton absorption peak of -CH₂- $\overset{|}{\underset{|}{\text{CH}}}$ -COONa, -CH₂-CH-CH₂-N⁺, -CH₂- $\overset{|}{\underset{|}{\text{CH}}}$ -CONH-, and -CH₂- $\overset{|}{\underset{|}{\text{CH}}}$ -CONH₂ in the branched chains. **Peak f** (δ2.33) was resulted from the proton absorption peak of >N-CH₂-CH₂-N< [41], $\overset{*}{\text{N}}\text{-CH}_2\text{-}$, and $\overset{*}{\text{N}}\text{-}\overset{\text{CH}_2\text{CH}_2\text{-CONH-}}{\underset{\text{CH}_2\text{CH}_2\text{-CONH-}}{\text{C}}}$ in the branched chain-skeleton and the proton absorption peak of -CH₂- $\overset{*}{\text{N}}\text{-CH}_2\text{CH}_2\text{-CONH-}$ and $\text{CH}_2\text{-CH-CH-COONa}$ at the branched chain. **Peak g** (δ3.04) was the proton absorption peak of CH- at the branched chain and the proton absorption peak of $\text{-CH}_2\text{-}\overset{\text{CH}_3}{\underset{\text{CH}_3}{\text{C}}}\text{-CH}_2\text{CH}_2(\text{CH}_2)_{15}\text{CH}_3$ at the hydrophobic branched chain of the DMCAAC-18 chain. The proton absorption peak of $\overset{*}{\text{N}}\text{-CH}_2\text{-CH}_2\text{-}$ at the branched chain skeleton, the proton absorption peak of -CH₂-CH₂-(CH₂)₁₅CH₃ in DMCAAC-18 chain, and the proton absorption peak of -CH₂SO₃Na in the AMPS chain resulted in **Peak h** (δ3.14). The proton absorption peak of $\text{-CH-CONHCH}_2\text{CH}_2\text{-}$ at the branched chain and the proton absorption peak of $\text{-N}^+\text{-}\overset{\text{CH}_3}{\underset{\text{CH}_3}{\text{C}}}\text{-CH}_2\text{-}$ in the DMCAAC-18 chain resulted in **Peak i** (δ3.38). **Peak j** (δ3.88) belonged to the proton absorption peak of $\text{CH-CONHCH}_2\text{-}$ and $\text{-CH}_2\text{-}\overset{*}{\text{N}}\text{-CH}_2\text{CH}_2\text{-CONH-}$ in the branched-chain and the proton absorption peak of $\text{-CH}_2\text{-}\overset{\text{CH}_2\text{-}}{\underset{\text{CH}_2\text{-}}{\text{N}}}\text{-}\overset{\text{CH}_2\text{-}}{\underset{\text{CH}_2\text{-}}{\text{N}}}\text{-CH}_2\text{-}$ in the branched chain-skeleton. **Peak k** (δ7.22) was the proton absorption peak of -CH₂- $\overset{|}{\underset{|}{\text{CH}}}$ -CONH₂ [63] in the branched chain. **Peak l** (δ8.01) was caused by the proton absorption peak of -CO-NH- at the branched chain and at the branched chain skeleton. The peaks corresponded to the expected chemical structure and functional group of HAPAM, demonstrating the successful synthesis of HAPAM.

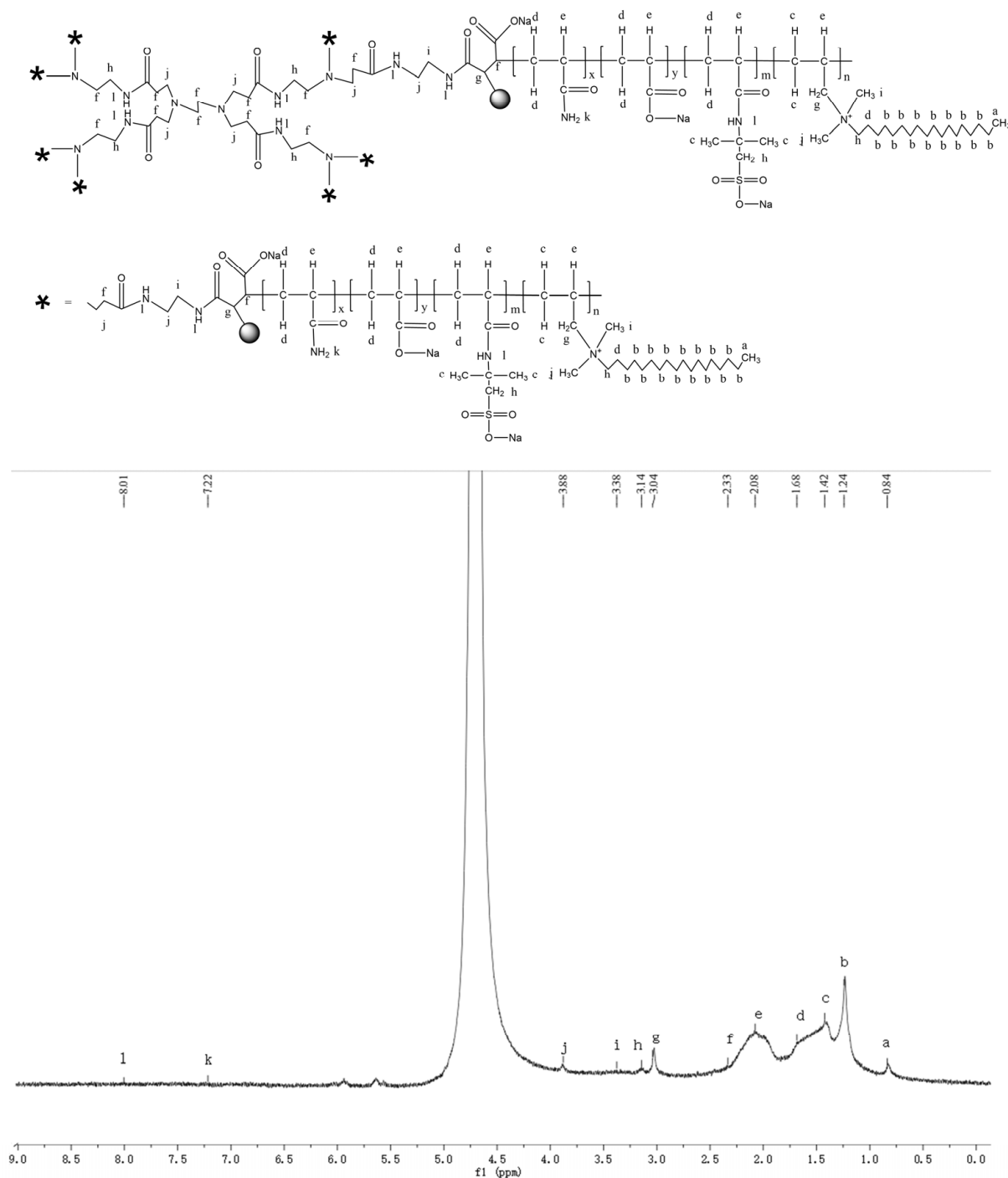


Figure 3. $^1\text{H-NMR}$ Spectrum of HAPAM.

The microstructure of PAM solution and HAPAM solution was observed by VEGA-3SBU scanning electron microscope. The SEM observations (magnifying $1000\times$ and $5000\times$) of HAPAM and PAM are shown in Figure 4. From the micro-scale structures visible in SEM, it can be found that the entanglement degree of complexes formed by the aggregation of many HAPAM polymers was significantly higher than that of PAM due to drying. In other words, compared to PAM, this phenomenon indicated that HAPAM had much denser networks, which was conducive to enhancing the rigidity and strength of molecular chains and molecular volume [64] and improving its shear resistance and sweep efficiency [65].

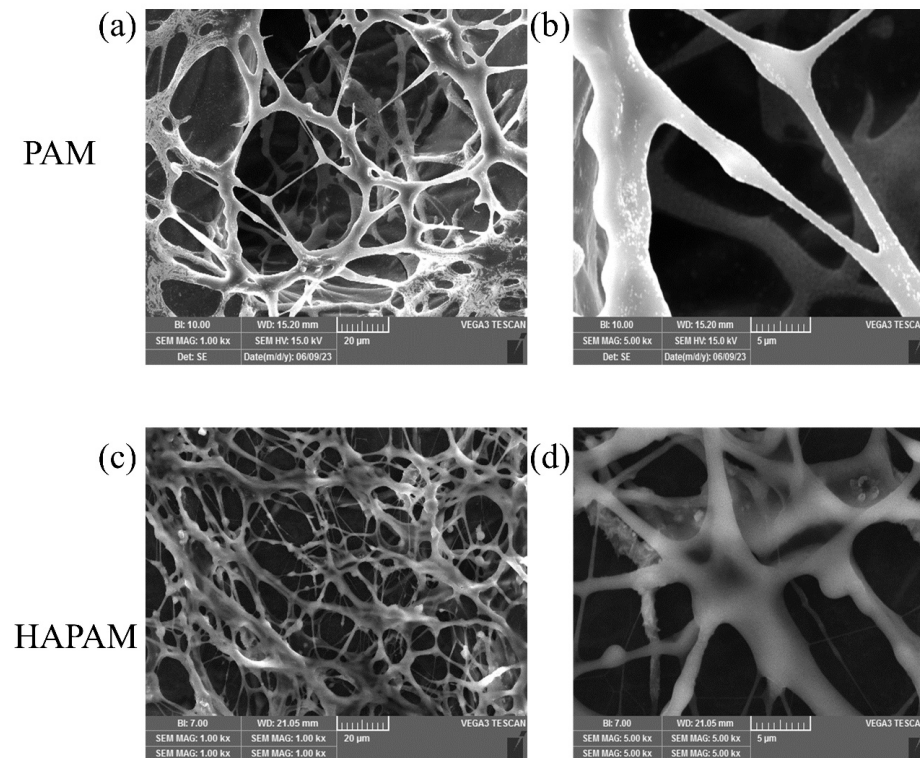


Figure 4. SEM observations of PAM ((a,b), magnifying $\times 1000$ and $\times 5000$) and HAPAM ((c,d), magnifying $\times 1000$ and $\times 5000$).

3.3. Determination of Intrinsic Viscosity and Molecular Weight

The molecular weight of a polymer can be measured from its intrinsic viscosity by a Ubbelohde viscometer at room temperature, which can be used to estimate the size of the polymer to better understand its hydrodynamic behavior. From the analysis of the structure of the synthesized hyperbranched HAPAM, it has similar branches to PAM. However, the linear and long molecular chains of HAPAM were distributed to the individual branches, reducing the fluid mechanical volume of the molecule. Thus, it can be theoretically estimated that the fluid mechanical volume of HAPAM was smaller than that of PAM. Additionally, 1 mol/L of NaCl was prepared with deionized water as the standard solution. 10 mL and 1 mol/L of NaCl solution was transferred into the Ubbelohde viscometer. The side vent tube was sealed, then the solution was gently sucked into the timing tube until the liquid reached about 5 mm above the upper timing mark. Then, loosen the side vent tube to allow the liquid to fall freely and measure the flow time. To measure the flow time, start the stopwatch when the meniscus drops below this upper timing mark, measuring the time for the meniscus to pass from the upper timing to the bottom timing mark (stop the stopwatch when the meniscus drops below the bottom timing mark). The average value of the three tests was taken as the flow time of the standard solution (10 mL and 1 mol/L of NaCl solution). Similarly, 10 mL of 500 mg/L polymer solutions (prepared with 1 mol/L of NaCl solution) was used to determine the flow time, as shown in Table 3. For a given capillary viscometry, it provides only a relative measure of the viscosity and not an absolute one, as shown in Equation (4). The intrinsic viscosity of the polymer can be obtained by extrapolating the plot of $\ln \eta_r / C$ vs. C to $C = 0$, as given in Equation (5). According to the general form of the Mark-Houwink relation, the Viscosity-average molecular weight of the polymer can be obtained in units g/mol by Equation (5).

$$\eta_r = \frac{\eta}{\eta_0} = \frac{t}{t_0} \quad (4)$$

$$[\eta] = \lim_{C \rightarrow 0} \left(\frac{1}{C} \frac{\eta}{\eta_0} \right) = KM^\alpha \quad (5)$$

η_r : relative viscosity, dimensionless; η ($\text{cm}^2 \text{s}^{-1}$) and t (s): viscosity and flow time of the polymer solution; η_0 ($\text{cm}^2 \text{s}^{-1}$) and t_0 (s): viscosity and flow time of NaCl standard solution; $[\eta]$: intrinsic viscosity, (cm^3/g); C : concentration of polymer solution, (g/cm^3); K : a constant of the Ubbelohde viscometer, ($\text{cm}^3 \text{mol}^{-1}$); M : the Viscosity-average molecular weight of polymer (g/mol); α : a dimensionless constant, ($0.5 < \alpha < 0.8$).

Table 3. Flow time measured by Ubbelohde viscometer.

Mass Concentrations	1st (s)	2nd (s)	3rd (s)	t_{average} (s)
1 mol/L of NaCl	112.9	112.6	112.7	112.7
500 mg/L of PAM + 1 mol/L of NaCl	167.2	167.3	167.5	167.3
500 mg/L of HAPAM + 1 mol/L of NaCl	143.5	143.8	143.6	143.6

According to experimental data and calculation, the intrinsic viscosity of PAM and HAPAM was $844 \text{ cm}^3/\text{g}$ and $500 \text{ cm}^3/\text{g}$, respectively. Meanwhile, the Viscosity-average molecular weight of PAM and HAPAM was $3.96 \times 10^6 \text{ g}/\text{mol}$ and $1.79 \times 10^6 \text{ g}/\text{mol}$, respectively. It is clear that the intrinsic viscosity and molecular weight of HAPAM were smaller than those of PAM. Due to the dendritic structure, the molecular chains of HAPAM were distributed over more branches, resulting in a smaller hydrodynamic volume per unit of polymer molecule in solution smaller than that of PAM. The smaller hydrodynamic volume possibly contributed to HAPAM having a stronger shear resistance at high speeds through small pores.

3.4. Thickening Capacity of HAPAM

The comparative thickening performance of HAPAM and PAM solutions with different concentrations is shown in Figure 5. It can be found that the overall trend of the apparent viscosity for both HAPAM and PAM solutions was increased with increasing mass concentrations. A noticeable thickening capacity behavior was observed for HAPAM. Specifically, after the mass concentration reached 1500 mg/L, the apparent viscosity of HAPAM was significantly increased with the mass concentration, and the apparent viscosity of HAPAM solution reached 590.86 mPa·s at the 2500 mg/L, which was about six times higher than that of PAM. The excellent thickening ability of HAPAM was caused by the fact that HAPAM has a spatial three-dimensional network structure and hydrophobic groups, which can be confirmed by SEM observations (Figure 4), $^1\text{H-NMR}$ (Figure 3), and IR spectrum (Figure 2). When the concentration of hydrophobic groups exceeded a specific concentration (critical association concentration) [66,67], the association of the main chains for HAPAM was gradually converted from intramolecular association to intermolecular association, resulting in a significant increase in the thickening capacity of HAPAM solution.

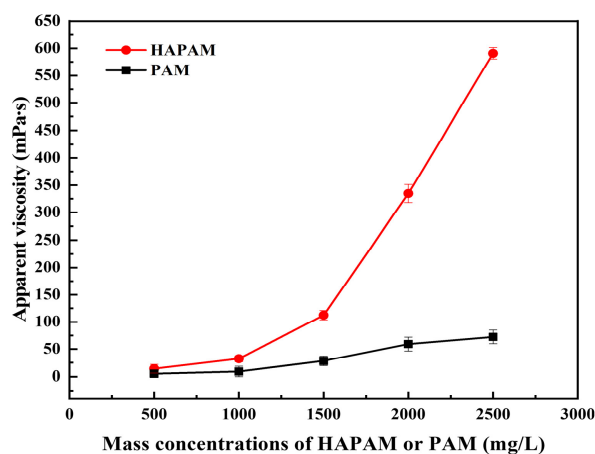


Figure 5. Thickening ability of HAPAM and PAM.

3.5. Shear-Resistance of HAPAM

HAPAM and PAM solutions prepared with mass concentrations of 500 mg/L, 1000 mg/L, 1500 mg/L, 2000 mg/L, and 2500 mg/L were sheared for 30 s using an XF crusher (Guangdong Xinfei Fashion Co., Shenzhen, China) at 20,000 r/min. After removing bubbles, the apparent viscosity of HAPAM and PAM solutions was measured before and after shearing at 65 °C. The shear-resistance and viscosity-retention of HAPAM and PAM solutions are shown in Figures 6 and 7, respectively. After 30 s shearing under the same experimental condition, the viscosity retention rate of PAM was about 60%, while HAPAM had a higher shear resistance with a viscosity retention rate of over 90%. The higher shear resistance of HAPAM may result from the highly entangled spatial three-dimensional network structure of HAPAM (as shown in Figure 4), which was greatly conducive to viscosity recovery and high viscosity retention rate.

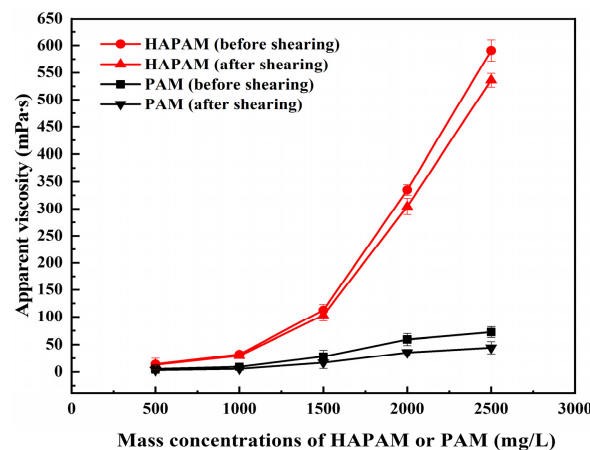


Figure 6. Shear-resistance of HAPAM and PAM.

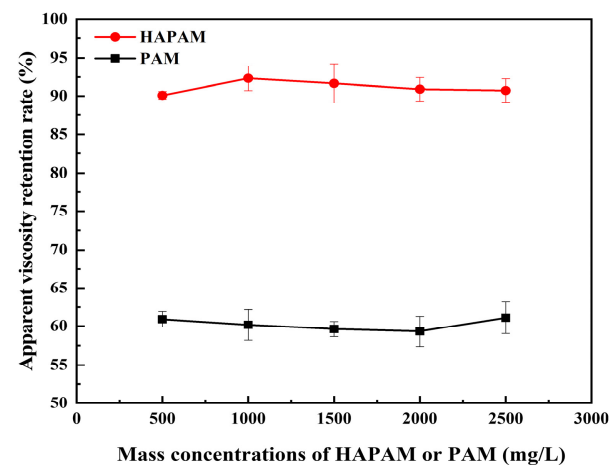


Figure 7. Viscosity-retention of HAPAM and PAM.

3.6. Temperature-Resistance of HAPAM

2000 mg/L of HAPAM and PAM solutions were stabilized at different temperatures for 24 h, and their apparent viscosity was measured, as shown in Figure 8. Clearly, it can be obtained that the apparent viscosity of both HAPAM and PAM solutions decreased with the increase of the temperature. Significantly, the apparent viscosity of both HAPAM and PAM solutions decreased slowly before 35 °C but rapidly decreased after 35 °C. Especially the apparent viscosity of the HAPAM solution was about 100 mPa·s at 65 °C, which was about 10 times higher than that of the PAM solution (12 mPa·s). This may be illustrated by the fact that the winding degree of HAPAM molecular chains was weakened by the enhancement of temperature. Since the mutual entanglement between macromolecular chains was caused

by the Brown motion of molecules. With the increase in temperature, the thermal motion of hydrophobic chains and water molecules was intensified, which damaged the entanglement between molecular chains to a certain extent, which was not conducive to hydrophobic association and thus reduced the viscosity. At low temperatures, the destructive effect of thermal motion was not obvious. After reaching a certain temperature, the damage of thermal motion rapidly weakened the winding degree of molecular chains. Thus, the viscosity decreased significantly. Comparatively, HAPAM displayed better temperature-resistance. The viscosity retention rate of HAPAM (59.1%) at 65 °C was higher than that of PAM (48.9%), which can enable us to demonstrate the temperature-resistance of HAPAM was better than that of PAM [68].

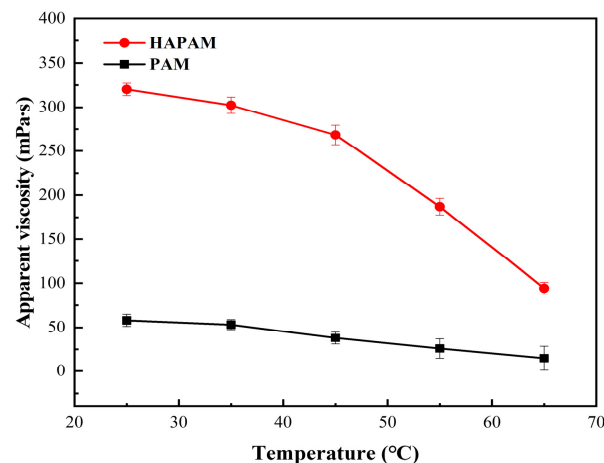


Figure 8. Temperature-resistance of HAPAM and PAM.

3.7. Salt-Resistance of HAPAM

2000 mg/L of HAPAM and PAM solutions were added with different kinds of salts (NaCl, CaCl₂, and MgCl₂) to investigate the salt resistance. Then, HAPAM and PAM solutions were stabilized at 65 °C for 30 min, and their apparent viscosity was measured. The comparative performance of salt resistance for HAPAM and PAM solutions is shown in Figure 9, respectively. Clearly, the apparent viscosity of PAM was rapidly decreased with the increase of salinity, and then it was kept at a low value. PAM was sensitive to salt, which was attributed to the fact that the presence of cations in the salt-containing solution played a shielding effect on the electricity of carboxylic acid groups generated from the hydrolysis of amide groups, weakening the electrostatic repulsion, resulting in the change of molecular chain from an extended state to a curled state. Therefore, the decrease of the hydrodynamic volume occupied in the space and the corresponding decrease in apparent viscosity of the PAM solution was observed [69]. However, at low salinity of HAPAM solution ($C_{CaCl_2} \leq 200$ mg/L and $C_{MgCl_2} \leq 200$ mg/L), the apparent viscosity of HAPAM solution gradually increased with the increase of the salinity, obtaining the maximum of 313.49 mPa·s (in CaCl₂ solution) and 338.69 mPa·s (in MgCl₂ solution), respectively. In the HAPAM solution, when added with salt, the association between molecular groups and molecular chains was shielded by ions, resulting in the enhancement of the interaction between solvent molecules. Hence, the molecular chains of HAPAM became stretched, which was favorable to the formation of hydrophobic micropores [70]. Therefore, the apparent viscosity did not decrease with the increase in the concentration of added salt but rather increased with the increase in the concentration of added salt. Meanwhile, at the high salinity of HAPAM solution ($C_{CaCl_2} > 200$ mg/L and $C_{MgCl_2} > 200$ mg/L), the apparent viscosity of HAPAM solution slowly decreased with the increase of the salinity degree. Clearly, compared with PAM, HAPAM exhibited better salt-tolerance-ability and long-term stability.

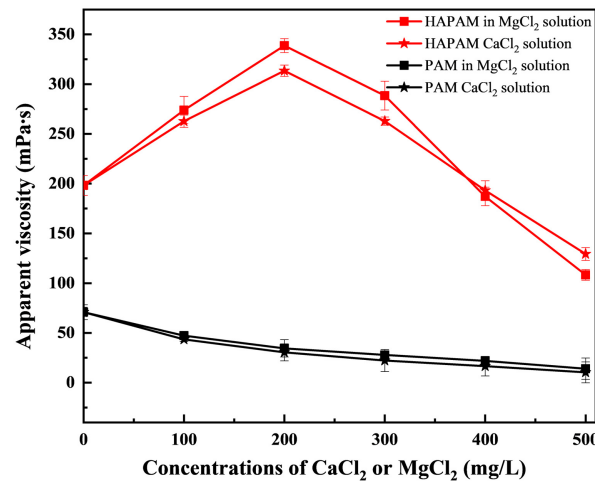


Figure 9. The salt-resistance of HAPAM and PAM in CaCl₂ and MgCl₂ solutions.

3.8. Interfacial Tension of HAPAM

HAPAM and PAM solutions (with mass concentrations of 500 mg/L, 750 mg/L, and 1000 mg/L) were prepared for measuring interfacial tension. The interfacial tensions were measured at the interface between crude oil and PAM or HAPAM solutions at 25 °C. As shown in Table 4, the interfacial tension for PAM or HAPAM solutions gradually decreased with the increase of its mass concentration. The decreased trend of interfacial tension of the oil | HAPAM interface was mainly ascribed to the directional distribution of the hydrophilic and lipophilic groups in the oil-polymer interface layer. As the concentration of HAPAM increased, the number of hydrophilic and lipophilic groups arranged on the interface layer increased, resulting in the greater ability to reduce the interfacial tension. Significantly, HAPAM exhibited a stronger ability to reduce the interfacial tension of the oil | HAPAM interface than that of PAM solution under the same experimental condition. Moreover, the amphiphilic property of HAPAM not only enables crude oil to be stripped from the surface of the porous medium but also effectively avoids chromatographic separation with excellent injectability and flow-controlling ability [71].

Table 4. Interfacial tension at the interface between HAPAM/PAM and crude oil.

Mass Concentrations	PAM	HAPAM
	Interfacial Tension (mN/m) ± Standard Deviations	
500 mg/L	22.94 ± 0.05	19.95 ± 0.02
750 mg/L	21.45 ± 0.05	18.64 ± 0.03
1000 mg/L	19.87 ± 0.03	15.84 ± 0.03

3.9. Resistance-Coefficient and Residual-Resistance-Coefficient of HAPAM

The resistance-coefficient (RF) and residual-resistance-coefficient (RFF) of PAM and HAPAM solutions (2000 mg/L) are shown in Table 4, respectively. RF and RFF were two important technical indicators for evaluating and understanding the oil-displacement mechanism of the polymers [72,73], which were also important indicators for indoor screening and evaluation of polymers. RF was used to describe the increase in water viscosity and retention due to the presence of polymer in the porous media. Moreover, for a low RF value, it implied that the polymer can be easily injected in the field without pressure increase concerns. Additionally, RFF was an indicator of the ability of polymer solution to reduce the permeability of pore media. The higher the RFF value, the more significant the adsorption and retention phenomenon of the polymer in porous media, which indicated the more helpful for improving the oil-displacing ability of the polymer. As given in Table 5, it can be obtained that the RF and RFF of PAM solutions (2000 mg/L) were 11.22 and 1.45, respectively. Similarly, the RF and RFF of HAPAM solutions were

16.77 and 2.80, respectively. Obviously, the RF and RFF of the HAPAM solution were higher than those of the PAM solution, so HAPAM should be superior to PAM in improving swept volume and building percolating resistance. The strong percolating resistance to the porous medium was readily facilitated by the high resistance coefficient of the HAPAM solution, allowing them to spread into more pores. Also, the permeability of the porous medium was greatly affected by the high residual resistance coefficient of the HAPAM solution, which can expand the coverage range of subsequent water flooding.

Table 5. Experimental parameters for measuring RF and RFF of HAPAM and PAM.

	Pressure in Water-Driving-Stage (MPa)	Pressure in Polymer-Flooding-Stage (MPa)	Pressure in Subsequent-Water-Driving-Stage (MPa)	RF	RFF
2000 mg/L of PAM	0.0094	0.1057	0.0137	11.22	1.45
2000 mg/L of HAPAM	0.0122	0.2049	0.0342	16.77	2.80

3.10. EOR of HAPAM Solutions

The oil-displacing performance of PAM and HAPAM solutions (2000 mg/L) is given in Figure 10. As the permeability of the sand pack core holder was approximately $0.293 \mu\text{m}^2$, following water cut to 95% for water flooding, the recovery efficiency increased with the increase of injection volume (PV) of the injected water. The recovery efficiency was about 56.43% at 3.2PV. During 3.2–3.6PV, using HAPAM solution at the same injection rate, the recovery efficiency was 60.00%, with an increase of 3.57%. The subsequent water flooding could further increase the oil recovery, reaching 69.46%, with an increase of 3.57%. Overall, the enhanced oil recovery (EOR) of PAM and HAPAM solutions was 9.29% and 13.03%, respectively. Obviously, HAPAM exhibited a stronger oil recovery ability than that of PAM. The higher EOR of HAPAM solution can be assigned to the improved sweep efficiency and sweep volume by the excellent thickening performance, shear-resistance, and hydrophobic association of HAPAM solution. In addition, HAPAM had surface activity to reduce the interfacial tension at the interface between the crude oil and HAPAM solution, which was also beneficial for improving oil washing efficiency.

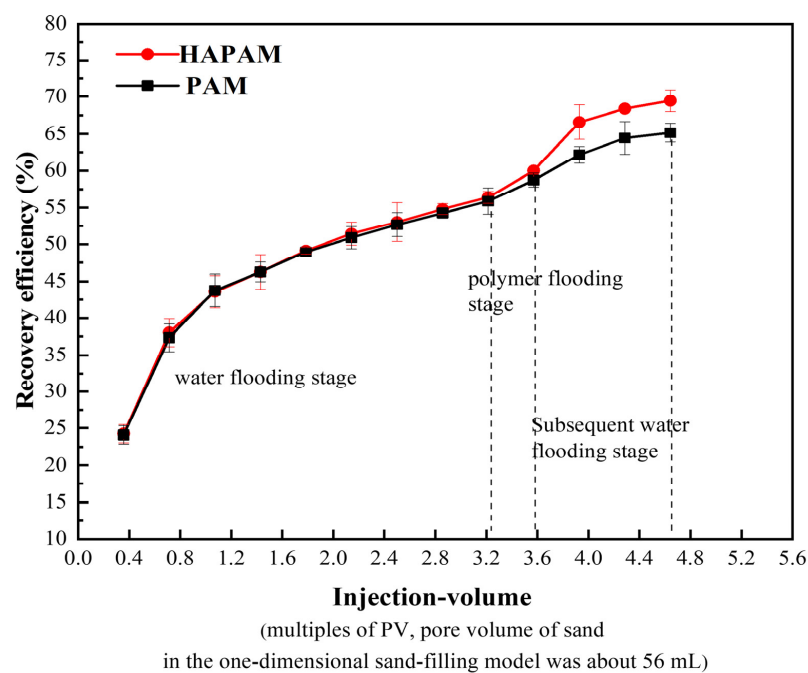


Figure 10. Variation of crude oil recovery rate with injection-volume during displacement of HAPAM and PAM (2000 mg/L).

4. Conclusions

In this study, a novel hyperbranched polymer with polyacrylamide side chains, HAPAM, was successfully synthesized by polymerization of AA, AM, AMPS, DMAAC-18, and M_{2.0} in aqueous solution at 40 °C and pH = 7 for 4 h, using (NH₄)₂S₂O₈-NaHSO₃ as initiator. The properties of HAPAM solution were superior to those of PAM solution, regarding thickening ability, shear-resistance, temperature-resistance, salt-resistance, the ability to reduce the interfacial tension between polymer solution and crude oil, and oil-displacement-efficiency. The excellent performance of HAPAM demonstrated the effectiveness and possibility of introducing hydrophobic groups (dimethyl octadecyl ammonium chloride, DMCAAC-18) and hydrophilic groups (AA, AM, and AMPS, abbreviated from 2-acrylamido-2-methyl-1-propanesulfonic acid) into the polymer chain to simultaneously enhance the shear-resistance and avoid the phenomenon of chromatographic separation. In addition, the successful synthesis of HAPAM and this novel synthetic scheme are important inspirations for the development of new high-performance oil-displacing agents.

Author Contributions: Methodology, X.Q.; Validation, Q.W. and X.Y.; Investigation, P.T.; Data curation, Q.W., H.Y., C.L., X.Y. and T.P.; Writing—original draft, Q.W.; Writing—review and editing, X.Q. and P.T.; Supervision, X.Q., C.L. and H.Y. All authors have read and agreed to the published version of the manuscript.

Funding: This work was supported by the Sichuan Key Technologies Research and Development Program (2023YFG0209) of Sichuan Provincial Department of Science and Technology, the Talent Introduction Project (2023R C21) of Sichuan University of Science and Engineering and the Open Project Program of Tianjin Key Laboratory of Brine Chemical Engineering and Resource Eco-utilization (No. BCERE202203).

Institutional Review Board Statement: Not applicable.

Informed Consent Statement: Not applicable.

Data Availability Statement: Data are contained within the article.

Acknowledgments: The authors would like to thank the Analytical Testing Center of Sichuan University of Science and Engineering for their assistance in the characterization of polymers.

Conflicts of Interest: Authors Hui Yang, Xiaoliang Yang and Tong Peng were employed by the company Jidong Oilfield Branch Company, PetroChina Company Limited. The remaining authors declare that the research was conducted in the absence of any commercial or financial relationships that could be construed as a potential conflict of interest.

References

1. Shuker, M.T.; Buriro, M.A.; Hamza, M.M. Enhanced oil recovery: A future for Pakistan. In Proceedings of the SPE/PAPG Annual Technical Conference, Islamabad, Pakistan, 3–5 December 2012; OnePetro: Richardson, TX, USA, 2012.
2. Gbadamosi, A.O.; Kiwalabye, J.; Junin, R.; Augustine, A. A review of gas enhanced oil recovery schemes used in the North Sea. *J. Pet. Explor. Prod. Technol.* **2018**, *8*, 1373–1387. [[CrossRef](#)]
3. Gbadamosi, A.; Patil, S.; Kamal, M.S.; Adewunmi, A.A.; Yusuff, A.S.; Agi, A.; Oseh, J. Application of polymers for chemical enhanced oil recovery: A review. *Polymers* **2022**, *14*, 1433. [[CrossRef](#)] [[PubMed](#)]
4. Agi, A.; Junin, R.; Jaafar, M.Z.; Sidek, M.A.; Yakasai, F.; Gbadamosi, A.; Oseh, J. Laboratory evaluation to field application of ultrasound: A state-of-the-art review on the effect of ultrasonication on enhanced oil recovery mechanisms. *J. Ind. Eng. Chem.* **2022**, *110*, 100–119. [[CrossRef](#)]
5. Malozyomov, B.V.; Martyushev, N.V.; Kukartsev, V.V.; Tynchenko, V.S.; Bukhtoyarov, V.V.; Wu, X.; Tyncheko, Y.A.; Kukartsev, V.A. Overview of methods for enhanced oil recovery from conventional and unconventional reservoirs. *Energies* **2023**, *16*, 4907. [[CrossRef](#)]
6. Sikiru, S.; Soleimani, H.; Yusuf, J.Y.; Hassan, Y.M.; Hamza, M.F.; Singh, R. Recent advance and prospect of enhanced oil recovery mechanisms in reservoir sandstone. *Preprints* **2023**, 2023091654.
7. Tahir, M.U.; Zhou, H.; Memon, B.S.; Liu, W.D.; Memon, A.; Khan, D.; Bakhsh, A. Comparative studies of enhancing oil recovery optimization for optimum oil field development. *Model. Earth Syst. Environ.* **2023**, *9*, 1477–1503. [[CrossRef](#)]
8. Gbadamosi, A.; Patil, S.; Al Shehri, D.; Kamal, M.S.; Hussain, S.S.; Al-Shalabi, E.W.; Hassan, A.M. Recent advances on the application of low salinity waterflooding and chemical enhanced oil recovery. *Energy Rep.* **2022**, *8*, 9969–9996. [[CrossRef](#)]

9. Jain, S.; Pachisia, H.; Sharma, A.; Patel, S.; Patel, S.; Ragunathan, B. A systematic review—Chemical EOR using surfactants and polymers. *Mater. Today Proc.* **2022**, *62*, 7220–7223. [[CrossRef](#)]
10. Mokheimer, E.M.; Hamdy, M.; Abubakar, Z.; Shakeel, M.R.; Habib, M.A.; Mahmoud, M. A comprehensive review of thermal enhanced oil recovery: Techniques evaluation. *J. Energy Resour. Technol.* **2019**, *141*, 030801. [[CrossRef](#)]
11. Hazarika, K. Chapter-8 classification of EOR technologies. In *Oil Recovery Principles & Practices*; CIIR Scientific Publications: Taipei, Taiwan, 2023; Volume 21.
12. Gray, L.; Goodyear, S. Overcoming the CO₂ supply challenge for CO₂ EOR. In Proceedings of the Abu Dhabi International Petroleum Exhibition and Conference, Abu Dhabi, United Arab Emirates, 10–13 November 2014; SPE: Kuala Lumpur, Malaysia, 2014; p. D021S032R005.
13. Núñez-López, V.; Moskal, E. Potential of CO₂-EOR for near-term decarbonization. *Front. Clim.* **2019**, *1*, 5. [[CrossRef](#)]
14. Khan, A.; Saxena, S.; Baloni, S.; Sharma, M.; Kodavaty, J. Overview and methods in enhanced oil recovery. *J. Phys. Conf. Ser.* **2021**, *2070*, 012061.
15. Abbas, A.H.; Sulaiman, W.R.W.; Jaafar, M.Z.; Gbadamosi, A.O.; Ebrahimi, S.S.; Elrufai, A. Numerical study for continuous surfactant flooding considering adsorption in heterogeneous reservoir. *J. King Saud Univ. Eng. Sci.* **2020**, *32*, 91–99. [[CrossRef](#)]
16. Levitt, D.B.; Pope, G.A. Selection and screening of polymers for enhanced-oil recovery. In Proceedings of the SPE Improved Oil Recovery Conference, Tulsa, OK, USA, 20–23 April 2008; SPE: Kuala Lumpur, Malaysia, 2008; p. SPE-113845-MS.
17. Pope, G.A. Recent developments and remaining challenges of enhanced oil recovery. *J. Pet. Technol.* **2011**, *63*, 65–68. [[CrossRef](#)]
18. Ayirala, S.; Sofi, A.; Li, Z.; Xu, Z. Surfactant and surfactant-polymer effects on wettability and crude oil liberation in carbonates. *J. Pet. Sci. Eng.* **2021**, *207*, 109117. [[CrossRef](#)]
19. Caili, D.; Qing, Y.; Fulin, Z.; Hanqiao, J. Residual polymer reutilization for IOR after polymer flooding: From laboratory to field application in daqing oilfield. *Pet. Sci. Technol.* **2011**, *29*, 2441–2449. [[CrossRef](#)]
20. Viken, A.L.; Spildo, K.; Reichenbach-Klinke, R.; Djurhuus, K.; Skauge, T. Influence of weak hydrophobic interactions on in situ viscosity of a hydrophobically modified water-soluble polymer. *Energy Fuels* **2018**, *32*, 89–98. [[CrossRef](#)]
21. Wang, S.; Shi, L.; Ye, Z.; Zhang, X.; Zhang, L.; Li, X. Experimental study on improving oil recovery in fluvial reservoir with polymer solutions. *AIP Adv.* **2021**, *11*, 055121. [[CrossRef](#)]
22. Wang, X.; Liu, W.; Shi, L.; Liang, X.; Wang, X.; Zhang, Y.; Wu, X.; Gong, Y.; Shi, X.; Qin, G. Application of a novel amphiphilic polymer for enhanced offshore heavy oil recovery: Mechanistic study and core displacement test. *J. Pet. Sci. Eng.* **2022**, *215*, 110626. [[CrossRef](#)]
23. Lei, T.; Wang, Y.; Zhang, H.; Cao, J.; Xiao, C.; Ding, M.; Chen, W.; Chen, M.; Zhang, Z. Preparation and performance evaluation of a branched functional polymer for heavy oil recovery. *J. Mol. Liq.* **2022**, *363*, 119808. [[CrossRef](#)]
24. Yao, T.; Liu, Q.; Liu, W.; Liu, F. Structural images of partially hydrolyzed polyacrylamide. *Acta Pet. Sin.* **2005**, *26*, 81.
25. Wenli, L.; Dong, H.; Li, W.; Qingxia, L.; Jian, F. Synthesis and property evaluation of a salt-and alkali-resistant star-polymer. *Pet. Explor. Dev.* **2010**, *37*, 477–482. [[CrossRef](#)]
26. Pu, W.-F.; Liu, R.; Li, B.; Jin, F.-Y.; Peng, Q.; Sun, L.; Du, D.-J.; Yao, F.-S. Amphoteric hyperbranched polymers with multistimuli-responsive behavior in the application of polymer flooding. *RSC Adv.* **2015**, *5*, 88002–88013. [[CrossRef](#)]
27. Lai, N.; Guo, X.; Zhou, N.; Xu, Q. Shear resistance properties of modified nano-SiO₂/aa/am copolymer oil displacement agent. *Energies* **2016**, *9*, 1037. [[CrossRef](#)]
28. Lai, N.; Zhang, Y.; Xu, Q.; Zhou, N.; Wang, H.; Ye, Z. A water-soluble hyperbranched copolymer based on a dendritic structure for low-to-moderate permeability reservoirs. *RSC Adv.* **2016**, *6*, 32586–32597. [[CrossRef](#)]
29. Duan, M.; Fang, S.; Zhang, L.; Wang, F.; Zhang, P.; Zhang, J. Shear degradation resistance of star poly(ethyleneimine)-polyacrylamides during elongational flow. *e-Polymers* **2011**, *11*, 86–99. [[CrossRef](#)]
30. Chen, Q.; Ye, Z.; Tang, L.; Wu, T.; Jiang, Q.; Lai, N. Synthesis and solution properties of a novel hyperbranched polymer based on chitosan for enhanced oil recovery. *Polymers* **2020**, *12*, 2130. [[CrossRef](#)]
31. Dong, L.; Li, Y.; Wen, J.; Gao, W.; Tian, Y.; Deng, Q.; Liu, Z. Functional characteristics and dominant enhanced oil recovery mechanism of polymeric surfactant. *J. Mol. Liq.* **2022**, *354*, 118921. [[CrossRef](#)]
32. Zhang, Q.; Mao, J.; Liao, Y.; Xu, T.; Zhang, H.; Du, A.; Yang, X.; Lin, C.; Mao, J. Evaluation of temperature resistance of non chemical crosslinked double-tailed hydrophobically associating polymer fracturing fluid. *React. Funct. Polym.* **2022**, *175*, 105268. [[CrossRef](#)]
33. Zhi, J.; Liu, Y.; Chen, J.; Jiang, N.; Xu, D.; Bo, L.; Qu, G. Performance evaluation and oil displacement effect of amphiphilic polymer heavy oil activator. *Molecules* **2023**, *28*, 5257. [[CrossRef](#)]
34. Zhu, Z.; Kang, W.; Sarsenbekuly, B.; Yang, H.; Dai, C.; Yang, R.; Fan, H. Preparation and solution performance for the amphiphilic polymers with different hydrophobic groups. *J. Appl. Polym. Sci.* **2017**, *134*. [[CrossRef](#)]
35. Zhao, Y.; Ke, Y.; Hu, X.; Peng, F. Synthesis, characterization and emulsification properties of an amphiphilic copolymer for enhanced oil recovery. *IOP Conf. Ser. Mater. Sci. Eng.* **2019**, *493*, 012121. [[CrossRef](#)]
36. Sui, Y.; Cao, G.; Guo, T.; Zhang, Z.; Zhang, Z.; Xiao, Z. Synthesis and mechanism study of temperature- and salt-resistant amphoteric polyacrylamide with MAPTAC and DTAB as monomers. *Processes* **2022**, *10*, 1666. [[CrossRef](#)]
37. Qin, X.; Zhu, S.; Shi, Q.; Li, C. Synthesis and properties of a dendrimer amphiphilic polymer as enhanced oil recovery chemical. *J. Chem.* **2023**, *2023*, 4271446. [[CrossRef](#)]

38. Shi, L.; Zhu, S.; Ye, Z.; Zhang, J.; Xue, X.; Zhao, W. The seepage flow characteristics of hydrophobically associated polymers with different aggregation behaviours in porous media. *R. Soc. Open Sci.* **2020**, *7*, 191270. [[CrossRef](#)]
39. Quan, H.; Li, Z.; Huang, Z. Self-assembly properties of a temperature- and salt-tolerant amphoteric hydrophobically associating polyacrylamide. *RSC Adv.* **2016**, *6*, 49281–49288. [[CrossRef](#)]
40. Shi, J.; Wu, Z.; Deng, Q.; Liu, L.; Zhang, X.; Wu, X.; Wang, Y. Synthesis of hydrophobically associating polymer: Temperature resistance and salt tolerance properties. *Polym. Bull.* **2022**, *79*, 4581–4591. [[CrossRef](#)]
41. Lai, N.; Qin, X.; Ye, Z.; Peng, Q.; Zhang, Y.; Ming, Z. Synthesis and evaluation of a water-soluble hyperbranched polymer as enhanced oil recovery chemical. *J. Chem.* **2013**, *2013*, 824785. [[CrossRef](#)]
42. Peng, H. Development and Performance Evaluation of a New Type of Low-Damage Fracturing Fluid. Master's Thesis, Southwest Petroleum University, Chengdu, China, 2014.
43. Izadi, M.; Mardani, H.; Roghani-Mamaqani, H.; Salami-Kalajahi, M.; Khezri, K. Hyperbranched poly (amidoamine)-grafted graphene oxide as a multifunctional curing agent for epoxy-terminated polyurethane composites. *ChemistrySelect* **2021**, *6*, 2692–2699. [[CrossRef](#)]
44. Lin, S.-Y.; Chu, H.-L. Fourier transform infrared spectroscopy used to evidence the prevention of β -sheet formation of amyloid β (1–40) peptide by a short amyloid fragment. *Int. J. Biol. Macromol.* **2003**, *32*, 173–177. [[CrossRef](#)] [[PubMed](#)]
45. Georges, R.; Freytes, M.; Hurtmans, D.; Kleiner, I.; Vander Auwera, J.; Herman, M. Jet-cooled and room temperature FTIR spectra of the dimer of formic acid in the gas phase. *Chem. Phys.* **2004**, *305*, 187–196. [[CrossRef](#)]
46. Yamamoto, M.; Sakurai, Y.; Hosoi, Y.; Ishii, H.; Kajikawa, K.; Ouchi, Y.; Seki, K. Softened CH stretching vibration of a long-chain n-alkane, n-C₄₄H₉₀, physisorbed on a Ag (111) surface: An infrared reflection absorption spectroscopic study. *J. Phys. Chem. B* **2000**, *104*, 7370–7376. [[CrossRef](#)]
47. Ahmad, H.; Hossain, M.E.; Rahman, M.A.; Rahman, M.M.; Miah, M.J.; Tauer, K. Carboxyl functionalized poly (methyl methacrylate-acrylic acid-ethylene glycol dimethacrylate) copolymer particles and their amination with amine-nucleophiles. *e-Polymers* **2008**, *8*, 96. [[CrossRef](#)]
48. Yilmaz, M.K. Palladium (II) complexes with new bidentate phosphine-imine ligands for the Suzuki CC coupling reactions in supercritical carbon dioxide. *J. Supercrit. Fluids* **2018**, *138*, 221–227. [[CrossRef](#)]
49. Lv, J.; Liu, S.; Feng, J.; Liu, Y.; Zhou, S.; Chen, R. Effective identification of paints pigments in hit-and-run cases with confocal Raman microscope. *Pigment Resin Technol.* **2016**, *45*, 294–300. [[CrossRef](#)]
50. Shanmugasundaram, A.; Krishnamoorthy, S. A systematically evolved method for the effective use of essential oil blends for the structural maintenance of palm leaf manuscripts. *J. Inst. Conserv.* **2024**, *47*, 82–98. [[CrossRef](#)]
51. Girma, W.; Diaz, I. Encapsulation of Co (II) complex with a schiff base ligands derived from 1, 10- phenantroline-5, 6-dione and o-phenylene diamine in zeolite y. *Int. J. Basic Appl. Sci.* **2015**, *1*, 35–41. [[CrossRef](#)]
52. Podstawka, E.; Światłowska, M.; Borowiec, E.; Proniewicz, L.M. Food additives characterization by infrared, Raman, and surface-enhanced Raman spectroscopies. *J. Raman Spectrosc.* **2007**, *38*, 356–363. [[CrossRef](#)]
53. Bahadur, A.; Shoaib, M.; Saeed, A.; Iqbal, S. FT-IR spectroscopic and thermal study of waterborne polyurethane-acrylate leather coatings using tartaric acid as an ionomer. *e-Polymers* **2016**, *16*, 463–474. [[CrossRef](#)]
54. Chen, Y.; Li, Y.; Chen, W.; Xu, W.W.; Han, Z.-k.; Waheed, A.; Ye, Z.; Li, G.; Baiker, A. Continuous dimethyl carbonate synthesis from CO₂ and methanol over Bi_xCe_{1-x}O₈ monoliths: Effect of bismuth do** on population of oxygen vacancies, activity, and reaction pathway. *Nano Res.* **2022**, *15*, 1366–1374. [[CrossRef](#)]
55. Fourneta, I.; Gall, E.A.; Deslandes, E.; Huvenne, J.-P.; Sombret, B.; Floc'h, J. In situ measurements of cell wall components in the red alga *Solieria chordalis* (Solieriaceae, Rhodophyta) by FTIR microspectrometry. *Bot. Mar.* **1997**, *40*, 45–48. [[CrossRef](#)]
56. Paradkar, M.; Irudayaraj, J. A rapid FTIR spectroscopic method for estimation of caffeine in soft drinks and total methylxanthines in tea and coffee. *J. Food Sci.* **2002**, *67*, 2507–2511. [[CrossRef](#)]
57. Ramis, G.; Larrubia, M.; Busca, G. On the chemistry of ammonia over oxide catalysts: Fourier transform infrared study of ammonia, hydrazine and hydroxylamine adsorption over iron–titania catalyst. *Top. Catal.* **2000**, *11*, 161–166. [[CrossRef](#)]
58. Yahaya, N.P.; Ali, I.; Modu, K.A.; Adamu, S. Adsorption study of methylene blue onto power activated carbon prepared from ananas comosus peels. *Nanochemistry Res.* **2023**, *8*, 231–242.
59. Huang, X.; Huang, D.; Ou, X.; Ding, F.; Chen, Z. Synthesis and properties of side-chain-type ion exchange membrane PEEK-g-StSO₃Na for bipolar membranes. *Appl. Surf. Sci.* **2012**, *258*, 2312–2318. [[CrossRef](#)]
60. Zhuang, J.; Li, M.; Pu, Y.; Ragauskas, A.J.; Yoo, C.G. Observation of potential contaminants in processed biomass using fourier transform infrared spectroscopy. *Appl. Sci.* **2020**, *10*, 4345. [[CrossRef](#)]
61. Bahraeian, S.; Abron, K.; Pourjafarian, F.; Majid, R.A. Study on synthesis of polypyrrole via chemical polymerization method. *Adv. Mater. Res.* **2013**, *795*, 707–710. [[CrossRef](#)]
62. Quan, H.; Lu, Q.; Chen, Z.; Huang, Z.; Jiang, Q. Adsorption–desorption behavior of the hydrophobically associating copolymer AM/APEG/C-18/SSS. *RSC Adv.* **2019**, *9*, 12300–12309. [[CrossRef](#)] [[PubMed](#)]
63. Salih, N.A. Synthesis of new heterocyclic compounds derived from anthrone and evaluation of their biological activity. *Synthesis* **2008**, *12*, 13. [[CrossRef](#)]
64. Sun, J.; Du, W.; Pu, X.; Zou, Z.; Zhu, B. Synthesis and evaluation of a novel hydrophobically associating polymer based on acrylamide for enhanced oil recovery. *Chem. Pap.* **2015**, *69*, 1598–1607. [[CrossRef](#)]

65. Jadhwar, P.; Saeed, M. Low salinity water and polymer flooding in sandstone reservoirs: Upscaling from nano-to macro-scale using the maximum energy barrier. *J. Pet. Sci. Eng.* **2023**, *220*, 111247. [[CrossRef](#)]
66. Ji, Y.; Wang, D.; Cao, X.; Guo, L.; Zhu, Y. Both-branch amphiphilic polymer oil displacing system: Molecular weight, surfactant interactions and enhanced oil recovery performance. *Colloids Surf. A Physicochem. Eng. Asp.* **2016**, *509*, 440–448. [[CrossRef](#)]
67. González Coronel, V.J.; Jiménez-Regalado, E.J. Rheological properties of three different microstructures of water-soluble polymers prepared by solution polymerization. *Polym. Bull.* **2011**, *67*, 251–262. [[CrossRef](#)]
68. Yang, H.; Zhang, H.; Zheng, W.; Li, X.; Wang, F.; Li, X.; Zhang, D.; Turtabayev, S.; Kang, W. Research on synthesis and salt thickening behavior of a binary copolymer amphiphilic polymer. *J. Pet. Sci. Eng.* **2021**, *204*, 108713. [[CrossRef](#)]
69. Jin, Z.; Shan, G.; Pan, P. Preparation and heat and salt resistance of AM/AMPS/SSS terpolymer. *CIESC J.* **2023**, *74*, 916–923. [[CrossRef](#)]
70. Wang, D.; Tan, J.; Han, Y.; Guo, Y.; An, H. Synthesis and properties of temperature-resistant and salt-tolerant tetra-acrylamide copolymer. *J. Macromol. Sci. Part A* **2019**, *56*, 1148–1155. [[CrossRef](#)]
71. Liu, Z.; Cheng, H.; Li, Y.; Li, Y.; Chen, X.; Zhuang, Y. Experimental investigation of synergy of components in surfactant/polymer flooding using three-dimensional core model. *Transp. Porous Media* **2019**, *126*, 317–335. [[CrossRef](#)]
72. Liang, K.; Han, P.; Chen, Q.; Su, X.; Feng, Y. Comparative study on enhancing oil recovery under high temperature and high salinity: Polysaccharides versus synthetic polymer. *ACS Omega* **2019**, *4*, 10620–10628. [[CrossRef](#)]
73. Bhatkar, S.; Kshirsagar, L.; Wadgaonkar, V.; Dulakhe, P.; Jhamtani, V. Application of chemical eor in viscous, heavy crude in thin stacked heterogeneous reservoirs using CMG simulator. *Pet. Coal* **2022**, *64*, 1000.

Disclaimer/Publisher's Note: The statements, opinions and data contained in all publications are solely those of the individual author(s) and contributor(s) and not of MDPI and/or the editor(s). MDPI and/or the editor(s) disclaim responsibility for any injury to people or property resulting from any ideas, methods, instructions or products referred to in the content.